CHEMISTRY
AN ASIAN JOURNAL
ACES
FULL PAPER

DOI: 10.1002/asia.201400051

Disassembly Kinetics of Quinone-Methide-Based Self-Immolative Spacers that Contain Aromatic Nitrogen Heterocycles

Ahmed Alouane,[a, b, c] Raphaël Labruère,*[a, b, c, e] Katherine J. Silvestre,[a, b] Thomas Le Saux,[c, d] Frédéric Schmidt,*[a, b] and Ludovic Jullien*[c, d]

Abstract: We prepared several pyridine- and pyrimidine-based self-immolative spacer groups to evaluate the significance of the resonance energy of the spacer aromatic ring on the kinetics of 1,4- and 1,6-elimination reactions, which govern spacer disassembly. Subsequently, we relied on a photoactivation procedure to accurately analyze the disassembly kinetics. Beyond providing new results that are relevant for deriving quantitative structure–property relationships, herein, we demonstrate that pH value can be used as an efficient parameter to finely control the disassembly time of a self-immolative spacer after an initial activation.

Keywords: kinetics · nitrogen heterocycles · photochemistry · pyrimidines · self-immolation

Introduction

First described by Katzenellenbogen and co-workers in 1981,[1] self-immolative spacer groups combine the cleavage of a covalent bond with the spontaneous release of one or several reporter groups.[2] More precisely, in these stimuli-responsive covalent chemical structures, a primary intramolecular reaction drives a second reaction, which releases a desired substrate (Scheme 1).[1]

Self-immolative spacer groups have now been extensively used in the design of prodrugs[3] and in bioanalysis.[4] Usefully, upon controlling the kinetics of substrate release after activation, these groups make it possible to spatially correlate the location of the activation position with substrate release. Hence, accurate kinetics analyses of the disassembly of self-immolative spacer groups have been critical in determining their scope of application. Useful structure–kinetics relationships have been established for the prediction of significant features, such as the stability of the covalent precursor and the rate of substrate release.[2a,5,6]

We have recently developed several procedures that rely on light activation to analyze the disassembly kinetics of self-immolative spacer groups down to a temporal resolution of 20 ms.[6] Our procedures have permitted us to analyze at different pH values and temperatures the disassembly kinetics of quinone-methide-based self-immolative spacers with 1) various electron-donating or -withdrawing substituents and 2) various links between the benzenic core and the substrate. For the purpose of comparison, we were interested in applying the same procedures to the investigation of pyridinone-methide elimination, which was previously described as effective.[7] In particular, we wondered whether fast disassembly could originate from the heteroaromatic ring[8] of the spacer and whether further acceleration could result from a further lowering of the resonance energy of the aromatic ring.[5d–e] Herein, we prepared several pyridine- and pyrimidine-based self-immolative spacer groups and analyzed the pH-dependent disassembly kinetics that were associated with their 1,4- and 1,6-eliminations.

[a] A. Alouane, Dr. R. Labruère, K. J. Silvestre, Dr. F. Schmidt
Institut Curie, Centre de Recherche
26 rue d'Ulm, Paris F-75248 (France)
Fax: (+33) 1-56-24-66-31
E-mail: frederic.schmidt@curie.fr

[b] A. Alouane, Dr. R. Labruère, K. J. Silvestre, Dr. F. Schmidt
CNRS, UMR 176
26 rue d'Ulm, Paris F-75248 (France)

[c] A. Alouane, Dr. R. Labruère, Dr. T. Le Saux, Prof. Dr. L. Jullien
Ecole Normale Supérieure, Département de Chimie
UMR CNRS-ENS-UPMC 8640 PASTEUR
24 rue Lhomond, 75231 Paris (France)
E-mail: ludovic.jullien@ens.fr

[d] Dr. T. Le Saux, Prof. Dr. L. Jullien
UPMC Univ. Paris 6
4 Place Jussieu, 75232 Paris (France)

[e] Dr. R. Labruère
Current address:
Institut de Chimie Moléculaire et
des Matériaux d'Orsay
UMR CNRS 8182, Université Paris Sud
Orsay, 91405 Cedex (France)
E-mail: raphael.labruere@u-psud.fr

Supporting information for this article is available on the WWW under http://dx.doi.org/10.1002/asia.201400051.

Results and discussion

Experimental Design

Herein, we synthesized a series of substituted-phenol-, pyridinol-, or pyrimidinol-containing caged spacers ($\mathbf{cS}^{\mathbf{X}}_{O,P}\mathbf{F}$) that could undergo *ortho* or *para* liberation through the cleavage of a carbamate bond. This functional group has been shown to be resistant to spontaneous hydrolysis (Scheme 2).

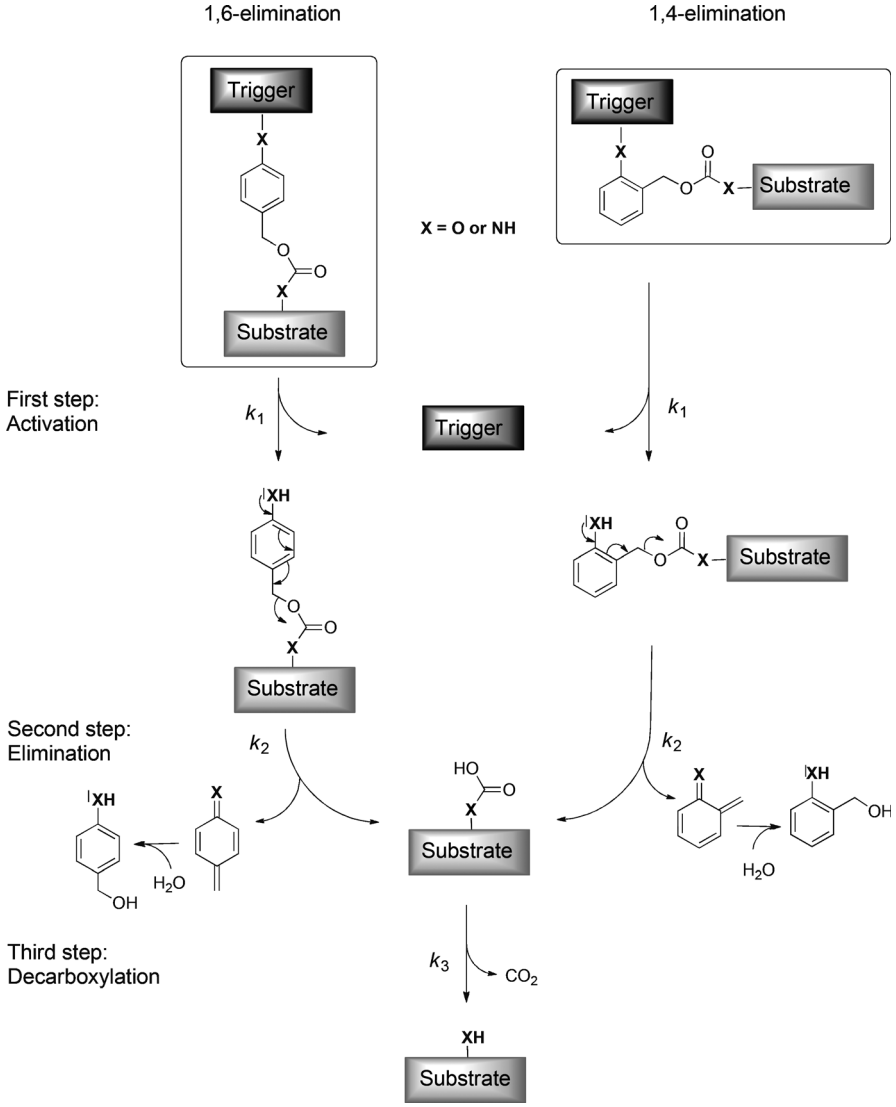

Scheme 1. In a quinone-methide-based self-immolative spacer, triggered cleavage spontaneously causes reorganization of the electron density within the aromatic core, which leads to the release of a substrate through 1,4- or 1,6-elimination. The quinone methide subsequently re-aromatizes in the presence of water.

To "lock" the precursor and permit its further photoactivation, the phenol oxygen atom was protected with the widely used 4,5-dimethoxy-2-nitrobenzyl caging group. Such 2-nitrobenzyl caging groups release phenols on the millisecond timescale, thereby making it possible to analyze self-immolation processes slower than 10 ms.[9] To analyze the stoichiometry and kinetics of self-immolation of the photoactivated spacers, we chose 7-amino-4-(trifluoromethyl)coumarin (**F**), a latent fluorophore for which the emission is quenched and blue-shifted in the caged precursor with respect to its strongly fluorescent free state.[10]

Synthesis

Caged self-immolative spacers $\mathbf{cS}^{\mathbf{X}}_{O,P}\mathbf{F}$ were synthesized in fair (30–46%; see the Supporting Information) yields by coupling of the caged benzyl-alcohol modules ($\mathbf{cS}^{\mathbf{X}}_{O,P}\mathbf{OH}$) to the reporting amino-coumarin through their corresponding isocyanate (Scheme 3).

Photoactivated Self-Immolation

All of the experiments were performed in MeCN/0.1 M Britton–Robinson buffer (1:1, v/v). From the absence of temporal evolution of the absorption spectrum on the 24 h timescale, we first concluded that the $\mathbf{cS}^{\mathbf{X}}_{O,P}\mathbf{F}$ molecules were stable in the dark under our experimental conditions. To analyze the self-immolation kinetics of the photoactivated $\mathbf{cS}^{\mathbf{X}}_{O,P}\mathbf{F}$ intermediates, we subsequently recorded the temporal evolution of the fluorescence emission from the reporting fluorophore upon submitting solutions of $\mathbf{cS}^{\mathbf{X}}_{O,P}\mathbf{F}$ to continuous 365 nm illumination to both photorelease and excite the reporting fluorophore. Our kinetic experiments were performed at various pH values (pH 4–10) to study the effect of the ionization state of the phenol spacer and the protonation of ring-nitrogen atoms on the rate of disassembly. Given the relevance of self-immolative spacers for biological applications, these assays were performed at 310 K.

First, we analyzed the behavior of phenyl reference compounds $\mathbf{cS}_O\mathbf{F}$ and $\mathbf{cS}_P\mathbf{F}$. From the temporal evolution of the fluorescence emission on the release of coumarin **F** upon the continuous illumination of 5 μM solutions of the samples at pH 8 (see the Supporting Information, Figure 2S), we confirmed the quantitative photorelease of **F** from $\mathbf{cS}_O\mathbf{F}$ and $\mathbf{cS}_P\mathbf{F}$ (see the Supporting Information).

A cascade of reactions leads from the photoactivated precursors ($\mathbf{cS}^{\mathbf{X}}_{O,P}\mathbf{F}$) to the final reporting fluorophore (**F**). As in our previous work, we adopted the kinetic model shown in Scheme 1, which contains steps that typically occur more slowly than on the millisecond timescale: First, illumination of the caged precursors yields phenol intermediates (rate constant k_1, associated with photoactivation), which subsequently disassemble into a benzenic core and a carbamic ester, which further decomposes to afford carbon dioxide and the reporting fluorophore in the third step (rate constants k_2 and k_3 refer to the self-immolation and decarboxy-

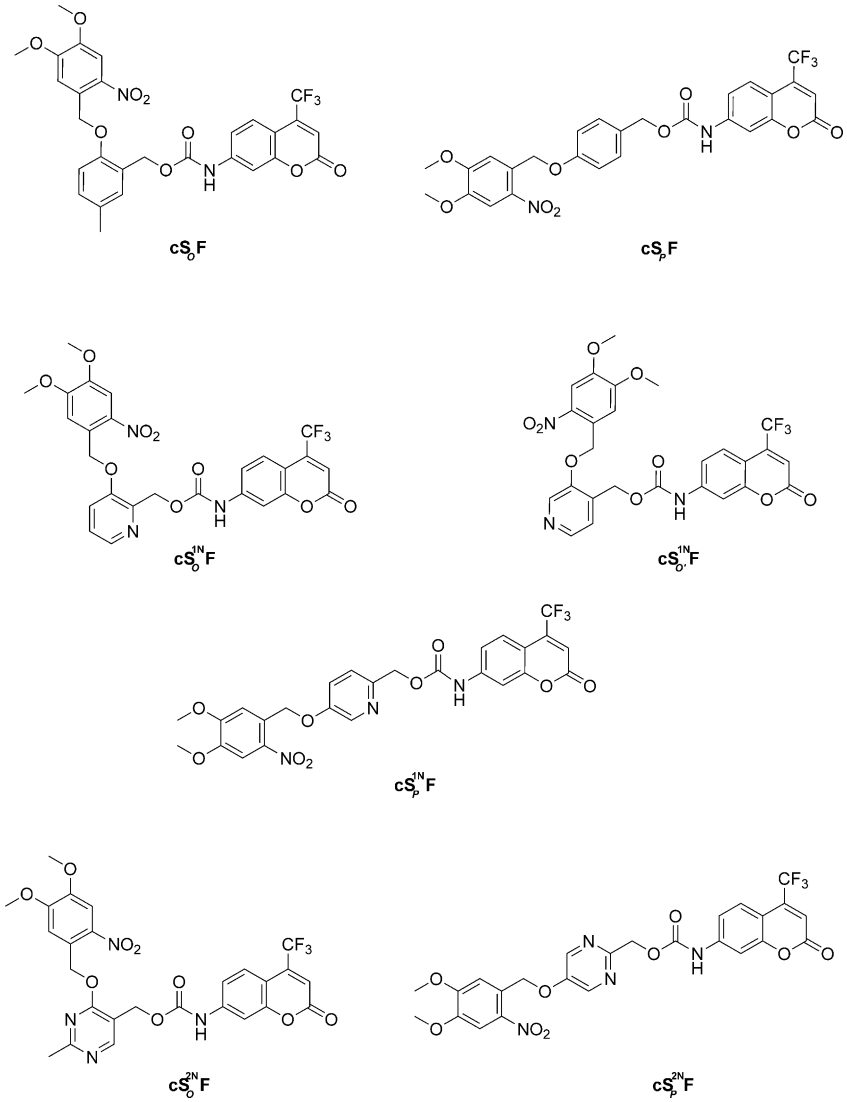

Scheme 2. Structures of caged self-immolative spacers $\mathbf{cS}^{\mathbf{X}}_{O,P}\mathbf{F}$.

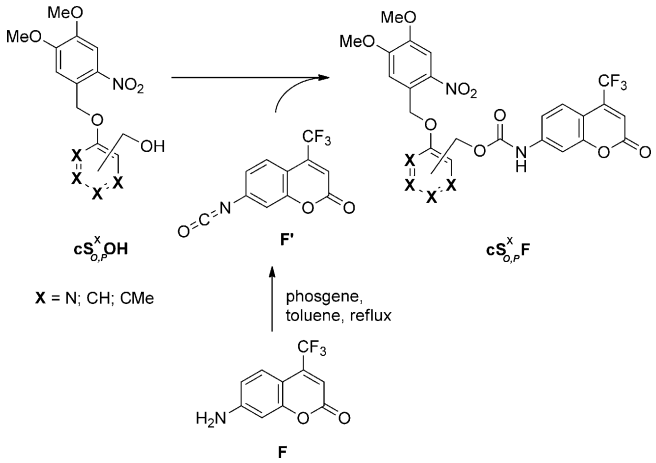

Scheme 3. Synthetic pathway for the synthesis of $\mathbf{cS}^{\mathbf{X}}_{O,P}\mathbf{F}$.

lation steps, respectively). Because the final step in this case was faster than the temporal resolution of our fluorescence-acquisition setup,[6b,11] we could analyze our data by using a simplified kinetic model that focused on the first two steps shown in Scheme 1 (see the Supporting Information).

The Supporting Information, Figure 2S, shows that our kinetic model was appropriate for obtaining satisfactory fits. Hence, for $\mathbf{cS}_P\mathbf{F}$, we could retrieve 1) the photoactivation quantum yield, $\phi(365\,\text{nm}) = 160(\pm1)\times10^{-4}$, which was in accordance with reported values for uncaging with the *ortho*-nitrobenzyl group;[12] 2) the relative brightness of the corresponding phenol intermediate with respect to that of coumarin **F**, 0.4, which was in line with our previous results;[6] 3) $k_2 = 0.6(\pm0.05)\,\text{s}^{-1}$ at 310 K. The corresponding values ($\phi(365\,\text{nm}) = 23.3(\pm0.2)\times10^{-4}$, 0.4, $k_2 = 0.4(\pm0.02)\,\text{s}^{-1}$) for $\mathbf{cS}_O\mathbf{F}$ have been reported previously.[6b] Table 1 summarizes the associated disassembly times, $\tau_d = 1/k_2$, for $\mathbf{cS}_O\mathbf{F}$ and $\mathbf{cS}_P\mathbf{F}$.

With these satisfactory results in hand, we analyzed the self-immolation kinetics of spacers that contained a pyridine core at pH 4 and 8. Figure 1 shows the temporal evolution of fluorescence emission from the continuous illumination of the three caged precursors $\mathbf{cS}^{\mathbf{1N}}\mathbf{F}$ at 310 K. As anticipated,

Table 1. Disassembly times (τ_d, in s) of the activated self-immolative spacers at several pH values. MeCN/0.1 M Britton–Robinson buffer (1:1, v/v), $T = 310$ K.

$\mathbf{cS}^{\mathbf{X}}_{O,P}\mathbf{F}$	pH 4	pH 8	pH 9.5
$\mathbf{cS}_O\mathbf{F}$	–	2.5(±0.1)	–
$\mathbf{cS}_P\mathbf{F}$	–	1.7(±0.3)	–
$\mathbf{cS}^{\mathbf{1N}}_O\mathbf{F}$	2702(±10)	149(±1)	–
$\mathbf{cS}^{\mathbf{1N}}_P\mathbf{F}$	8330(±50)	294(±2)	–
$\mathbf{cS}^{\mathbf{1N}}_{O'}\mathbf{F}$	1515(±3)	1667(±5)	–
$\mathbf{cS}^{\mathbf{2N}}_P\mathbf{F}$	–[a]	7690(±30)	1429(±7)[b] 1250(±10)[c]
$\mathbf{cS}^{\mathbf{2N}}_O\mathbf{F}$	–[a]	1587(±2)	250(±2)[b] 204(±3)[c]

[a] No discernible release of **F** under the experimental conditions; [b] values extracted from the experiments at constant pH value; [c] values extracted from the two-stage (pH 4 to 9.5) experiments.

an increase in fluorescence emission was observed, which was associated with the photorelease of the strongly fluorescent coumarin **F**, but also possibly of the intermediates shown in Scheme 1. In particular, by using a solution of **F** for the fluorescence-emission calibration, the final signal notably compared with the one expected from the quantitative photorelease of **F** (Figure 1). In that series, the caged compounds again led to satisfactory fits and demonstrated extracted values of the photoactivation quantum yields, ϕ-(365 nm), that were in line with literature expectations at both investigated pH values;[12] k_2 values were within the range $1–60\times10^{-4}\,s^{-1}$, with the smallest values observed at pH 4. The disassembly times, $\tau_d=1/k_2$, are shown in Table 1.

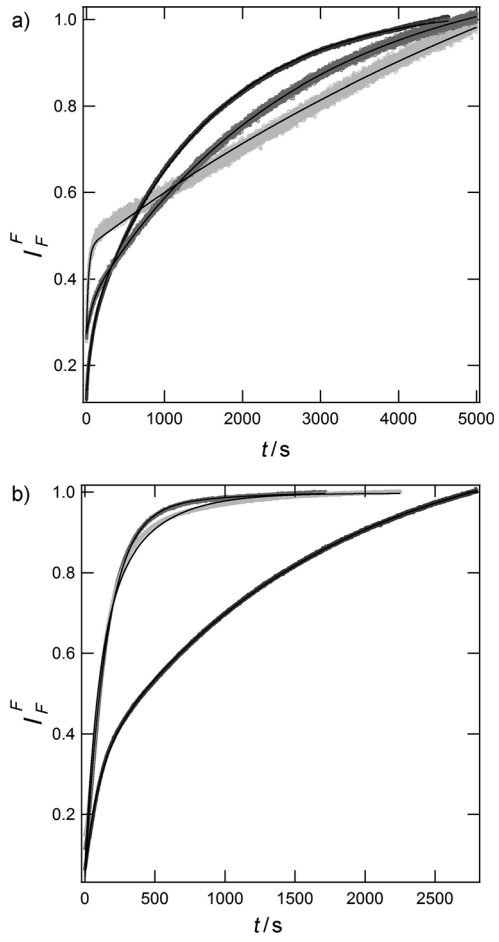

Figure 1. Temporal evolution of the fluorescence emission, $I_F^F(t)$ ($\lambda_{em}=$ 500 nm), at pH 4 (a) and pH 8 (b) upon illumination at $\lambda_{ex}=365(\pm25)$ nm a solution of $\mathbf{cS_O^{1N}F}$ (4(±1) μM; gray), $\mathbf{cS_P^{1N}F}$ (3(±0.8) μM; light gray), and $\mathbf{cS_{O'}^{1N}F}$ (2.5(±0.5) μM; black) at a light intensity of $18.9(\pm0.5)\times10^{-9}$ Ein s^{-1}. Markers denote experimental data; solid lines indicate fits to [Eq. (33)]. From the signal calibration with the fluorophore (**F**), we extracted final coumarin concentrations ($\boldsymbol{F}_\infty$) of 2(±1), 1.5(±1), and 1.7(±1) μM (a) and 3(±1), 2(±1), and 1.5(±1) μM (b) for $\mathbf{cS_O^{1N}F}$, $\mathbf{cS_P^{1N}F}$, and $\mathbf{cS_{O'}^{1N}F}$, respectively. From these fits, we also obtained: $\mathbf{cS_O^{1N}F}$: $\phi=78(\pm0.5)\times10^{-4}$, $k_2=0.00037(\pm0.00003)\,s^{-1}$ (pH 4), and $0.0067(\pm0.0003)\,s^{-1}$ (pH 8); $\mathbf{cS_P^{1N}F}$: $\phi=62.2(\pm0.4)\times10^{-4}$, $k_2=0.00012(\pm0.00007)\,s^{-1}$ (pH 4), and $0.0034(\pm0.0006)\,s^{-1}$ (pH 8); $\mathbf{cS_{O'}^{1N}F}$ $\phi=48.5(\pm0.5)\times10^{-4}$, $k_2=0.00066(\pm0.00005)\,s^{-1}$ (pH 4), and $0.0006(\pm0.00002)\,s^{-1}$ (pH 8). Solvent: MeCN/0.1 M Britton–Robinson buffer (pH 4, pH 8; 1:1, v/v), $T=310$ K.

The corresponding experiments and analyses were also performed for the caged self-immolative spacers that contained a pyrimidine core. At pH 8 and 9.5, illumination of solutions of $\mathbf{cS_P^{2N}F}$ and $\mathbf{cS_O^{2N}F}$ led to the complete liberation of **F** (Figure 2a,b). However, in contrast to the phenyl and pyridine series, the release of coumarin **F** did not occur at pH 4. Indeed, the emission spectra that was recorded after the longest investigated times did not match the emission spectrum of coumarin **F**, but rather was in agreement with the expected blue-shifted ones of carbamic intermediates $\mathbf{S_P^{2N}F}$ and $\mathbf{S_O^{2N}F}$ (Figure 2a,b). This assumption was confirmed by HPLC with mass spectrometry detection: At pH 4, illumination of $\mathbf{cS_P^{2N}F}$ led to the disappearance of the signal for $\mathbf{cS_P^{2N}F}$ and the emergence of a peak when detection was performed for the $\mathbf{S_P^{2N}F}$ molecular weight (see the Supporting Information).

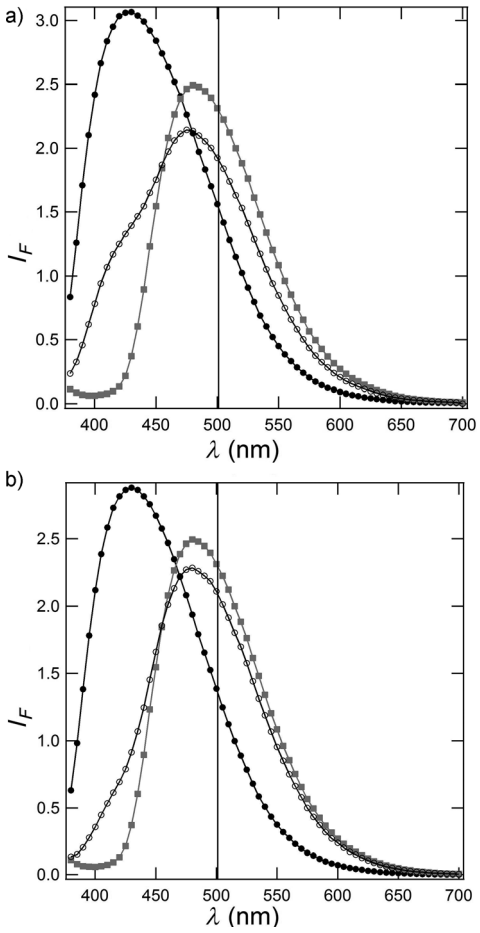

Figure 2. Final emission spectra that result from photoactivation of caged self-immolative spacers $\mathbf{cS_P^{2N}F}$ (a) and $\mathbf{cS_O^{2N}F}$ (b). The fluorescence emission spectra ($\lambda_{ex}=365$ nm) were recorded for 5(±0.1) μM **F** (squares; identical shape at pH 4 and 9.5) or 5(±1) μM solutions of $\mathbf{cS_{OP}^{2N}F}$ after complete photoactivation at pH 4 (disks) and 9.5 (circles). Solvent: MeCN/0.1 M Britton–Robinson buffer (1:1, v/v), $T=310$ K. In line with the deactivation of the nitrogen atom of the carbamic group, the final emission spectrum at pH 4 is blue-shifted with respect to the **F** emission spectrum at the same pH value. In contrast, except for a shoulder that originated from the remaining intermediate, $\mathbf{S_{OP}^{2N}F}$, the final emission spectrum at pH 9.5 matched the **F** spectrum.

To further test the hypothesis that $\mathbf{cS}^{\mathbf{2N}}_{O,P}\mathbf{F}$ could not self-immolate at pH 4, we devised a complementary illumination experiment: We recorded the temporal evolution of the fluorescence emission at pH 4 and subsequently increased the pH value of the solution to 9.5 by adding concentrated sodium hydroxide (Figure 3a,b). Before the pH increase, we observed a monoexponential relaxation, in line with uncaging leading to the formation of $\mathbf{S}^{\mathbf{2N}}_{O,P}\mathbf{F}$. We extracted $\phi(365\text{ nm}) = 16.2(\pm0.2)\times10^{-4}$ and $18.3(\pm0.7)\times10^{-4}$ for the photoactivation quantum yields of $\mathbf{cS}^{\mathbf{2N}}_{P}\mathbf{F}$ and $\mathbf{cS}^{\mathbf{2N}}_{O}\mathbf{F}$, respectively, in line with the values observed above. After the pH increase, we also observed a monoexponential relaxation, which was expected for the decomposition of $\mathbf{S}^{\mathbf{2N}}_{O,P}\mathbf{F}$ into the aromatic core, coumarin **F**, and carbon dioxide, assuming that the decomposition of the carbamic intermediate was fast.[6b,11] Moreover, the final emission spectrum was consistent with the quantitative liberation of coumarin **F**.

Following the above interpretation, we analyzed the temporal evolution of the fluorescence emission from illuminated solutions of $\mathbf{cS}^{\mathbf{2N}}_{O,P}\mathbf{F}$ at constant pH value. At pH 4, the experimental curves were successfully fitted by using a one-step kinetic model (see the Supporting Information, Figure 5S), thereby yielding $\phi(365\text{ nm}) = 16.2(\pm0.2)\times10^{-4}$ and $18.3(\pm0.7)\times10^{-4}$ for the photoactivation quantum yields of $\mathbf{cS}^{\mathbf{2N}}_{P}\mathbf{F}$ and $\mathbf{cS}^{\mathbf{2N}}_{O}\mathbf{F}$, respectively, which were in good agreement with the values obtained in the pH-jump experiments. In contrast, at pH 8 and 9.5, we employed the kinetic model that involved the two first steps shown in Scheme 1 to fit the experimental data. Hence, by using 0.5 for the relative brightness of the corresponding phenol intermediate with respect to that of coumarin **F** for both compounds, we obtained $\phi(365\text{ nm}) = 20.9(\pm0.5)\times10^{-4}$ and $18.3(\pm0.7)\times10^{-4}$ and $0.7(\pm0.09)\times10^{-3}$ and $4(\pm0.5)\times10^{-3}\text{ s}^{-1}$ for the photoactivation quantum yields and k_2 values at 310 K for $\mathbf{cS}^{\mathbf{2N}}_{P}\mathbf{F}$ and $\mathbf{cS}^{\mathbf{2N}}_{O}\mathbf{F}$, respectively. In particular, the latter values were in line with those extracted from the pH-jump experiments. Table 1 lists the extracted disassembly times.

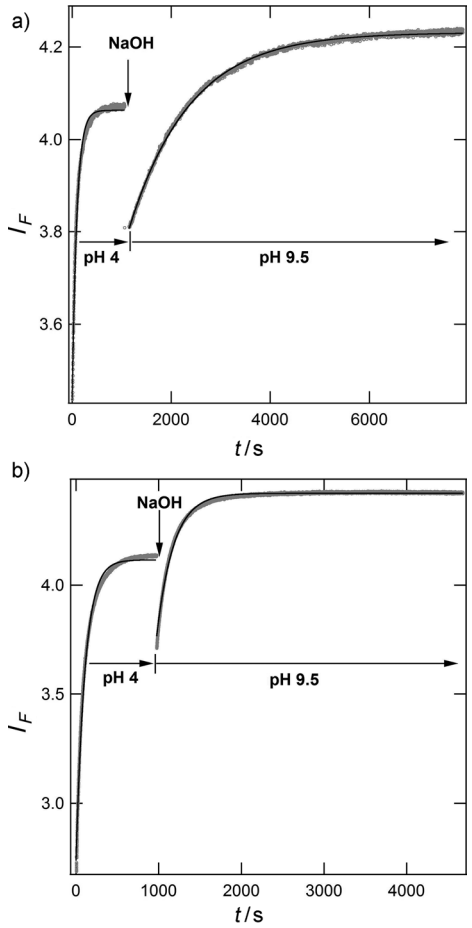

Figure 3. Inhibition of total disassembly after photoactivation of caged self-immolative spacers $\mathbf{cS}^{\mathbf{2N}}_{P}\mathbf{F}$ (a) and $\mathbf{cS}^{\mathbf{2N}}_{O}\mathbf{F}$ (b) at pH 4. Temporal evolution of the fluorescence emission at $\lambda_{em} = 500$ nm upon illumination of a) 5(±1) μM·$\mathbf{cS}^{\mathbf{2N}}_{P}\mathbf{F}$ or b) 2.5(±0.5) μM $\mathbf{cS}^{\mathbf{2N}}_{O}\mathbf{F}$ solutions at $\lambda_{ex} = 365$-(±25) nm, 18.9×10^{-9} Ein s^{-1}. After reaching a steady-state at pH 4, the pH value was raised to pH 9.5 by the addition of NaOH. Markers denote the experimental data; solid lines indicate fits with [Eq. (34)] at pH 4 and with [Eq. (34)] at pH 9.5 (see the Supporting Information). Solvent: MeCN/0.1 M Britton–Robinson buffer (1:1, v/v), $T = 310$ K.

Discussion

This investigation was conceived to evaluate the relevance of heteroaromatic rings for designing faster self-immolative spacers that relied on quinone-methide-like elimination. The rationale behind the choice of the pyridine and pyrimidine rings was their significantly lower resonance energies (142 and 132 kJ mol^{-1}) than 150 kJ mol^{-1} for the benzene ring.[16] Indeed, disassembly of the phenol intermediates ($\mathbf{S}^{\mathbf{X}}_{O,P}\mathbf{F}$) requires loss of aromaticity and the corresponding energy barrier should be lowered by decreasing the resonance energy so as to accelerate spacer disassembly.

For data analysis, it is first essential to compare behaviors at a same ionization state. Indeed, we have previously reported that phenol ionization significantly decreases the disassembly time in the phenyl series.[6b] The pK_a values of the phenol group in the phenyl cores of $\mathbf{cS}_{O}\mathbf{F}$ and $\mathbf{cS}_{P}\mathbf{F}$ are above 10;[6b] thus, that only the phenol group is present at the investigated pH value (pH 8). In 3-hydroxypyridine, the reported pK_a values that are associated to the ring-nitrogen atom and the phenol group can be estimated to be about 5.0 and 8.5.[7,13] Correspondingly, experiments at pH 4, 8, and 9.5 would involve phenol pyridinium, phenol pyridine, and phenolate pyridine cores, respectively. The pK_a values for ring-nitrogen atoms in the unsubstituted pyrimidinol core have been reported to be about −7.0 and 1.5,[14] whereas the phenol pK_a values were estimated to be 7.0[13] and 8.6[14b,15] in the bare pyrimidinol cores $\mathbf{S}^{\mathbf{2N}}_{P}$ and $\mathbf{S}^{\mathbf{2N}}_{O}$, respectively. Thus, the pyrimidinol core should always contain unprotonated nitrogen atoms under our experimental conditions. In contrast, it would involve the phenol group at pH 4 but the phenolate from pH 8 and above.

First, we will focus on the effect of the structure of the aromatic ring on the disassembly time of the neutral self-immolative spacer. Thus, we will compare the data for the phenyl and pyridine series at pH 8 with the data for the pyrimidine series at pH 4. Self-immolative spacers with a benzene core displayed faster release than those with a pyridine

core; the pyrimidinic spacers did not self-immolate on the investigated timescale under such conditions. Beyond the considerations based on resonance energy (which would have led us to expect the reverse order), we hypothesize that this result originates from differences in the electron density on the carbon atom bearing the benzylic substituent that is involved in the elimination step. The electron-withdrawing nitrogen atom is expected to decrease this density in $\mathbf{cS}_{O}^{1N}\mathbf{F}$ and $\mathbf{cS}_{O'}^{1N}\mathbf{F}$ with respect to $\mathbf{cS}_{O}\mathbf{F}$ and in $\mathbf{cS}_{P}^{1N}\mathbf{F}$ with respect to $\mathbf{cS}_{P}\mathbf{F}$. This feature should lead to longer disassembly times. In particular, such an explanation could be strengthened by the observation that 1) nitrogen protonation leads to further slowdown of the disassembly in the pyridine series at pH 8; 2) the presence of two nitrogen atoms on the aromatic ring effectively suppresses disassembly, as observed in the pyrimidine series at pH 4.

Next, we will analyze the effect of spacer ionization on the disassembly rate. As we previously observed for the phenyl series,[6b] phenol ionization significantly accelerated disassembly for the pyrimidine series; on increasing the pH value from 8 to 9.5, we typically observed a decrease in the disassembly time by a factor of 5. This observation confirmed the trend that electron-rich aryl cores accelerated self-immolation.[5,6b–c]

Finally, we will examine the role of *ortho*/*para* substitution on the elimination rate. In agreement with previous observations,[17] *ortho*- and *para*-quinone-methide elimination occurred on similar timescales (cf. $\mathbf{cS}_{O}\mathbf{F}$ and $\mathbf{cS}_{P}\mathbf{F}$). We arrived at the same conclusion regarding pyridinone-methide elimination (cf. $\mathbf{cS}_{O}^{1N}\mathbf{F}$ and $\mathbf{cS}_{P}^{1N}\mathbf{F}$). However, one should note that we observed that the disassembly times of two *ortho*-substituted derivatives differed by a factor of about 10 (cf. $\mathbf{cS}_{O}^{1N}\mathbf{F}$ and $\mathbf{cS}_{O'}^{1N}\mathbf{F}$), which revealed the importance of the position of the nitrogen atom on the aromatic core. Unlike $\mathbf{cS}_{O}^{1N}\mathbf{F}$, $\mathbf{cS}_{O'}^{1N}\mathbf{F}$ showed a relatively slow release that was not influenced by protonation. In that case, the exocyclic methylene group that contained the leaving group was at the *para* position relative to the ring-nitrogen (Scheme 2). Thus, we hypothesized that the neutral pyridinic nitrogen moiety of $\mathbf{cS}_{O}^{1N}\mathbf{F}$ at the *ortho* position relative to the benzylic position could assist the liberation of the reporter because the nitrogen lone pair could attack the electrophilic carbonyl group of the carbamate linkage.

Conclusions

Pyridine- and pyrimidine-based self-immolative spacer groups have been shown to disassemble through 1,4- and 1,6-elimination pathways. A photoactivation procedure has been used to show that these self-immolative spacers exhibited slower kinetics for spacer disassembly than their corresponding benzenic analogues. These results are relevant for deriving quantitative structure–property relationships. In particular, they suggest that electron density plays a more important role than resonance energy in governing the disassembly rate of an aromatic ring spacer. Interestingly, the observed pH-dependence of the disassembly time for this series of self-immolative spacers could be significant for various applications, ranging from prodrugs to the programmed degradation of materials.

Experimental Section

General Synthesis

Commercially available chemicals were used without further purification. Anhydrous solvents were freshly distilled prior to use. Low-actinic glassware was used for all experiments with compounds that contained nitroveratryl moieties. Column chromatography was performed on Merck silica gel 60 (0.040–0.063 mm). Analytical and thin layer chromatography (TLC) were performed on plates that were precoated with Merck silica gel 60 F-254; detection was performed by using UV light ($\lambda = 254$ nm). NMR spectra were recorded on an AC Bruker spectrometer at 300 MHz (for ^{1}H nuclei) and 75 MHz (for ^{13}C nuclei). Coupling constants (J) are in Hz. HPLC analysis and purification of the final caged species were performed on a Waters system with a Wdelta 600 pump and a PDA 996 UV detector at $\lambda = 245$ nm (analytical HPLC: X-Terra Waters MS C18 5 mm (particle size) column, 150 mm (length) × 4.6 mm (diameter), flow rate = 1 mL min^{-1}; preparative HPLC: X-Terra Waters Prep MS C18 5 mm (particle size) column, 150 mm (length) × 19 mm (diameter), flow rate = 10 mL min^{-1}; elution with MeCN/water mixtures). For the synthesis of the intermediate benzylic alcohols, $\mathbf{cS}_{O,P}^{X}\mathbf{OH}$, see the Supporting Information.

*7-Isocyanato-4-(trifluoromethyl)-2 H-chromen-2-one (**F′**)*

To a suspension of 7-amino-4-(trifluoromethyl)-2*H*-chromen-2-one (**F**, 100 mg, 0.4 mmol) under an Ar atmosphere was dropwise added a 20% solution of phosgene in toluene (4 mL, 8 mmol) with a syringe. The reaction mixture was heated at reflux for 15 h under an Ar atmosphere, during which time a white solid precipitated out of the solution. After cooling, Ar gas was bubbled through the solution for 15 min to remove any unreacted phosgene. Then, the reaction mixture was evaporated under reduced pressure to afford the product as a white solid (100 mg, 90% yield), which was used directly in the next step.

General Procedure for the Preparation of Caged Self-Immolative Spacers

To a solution of the desired benzyl alcohol intermediate ($\mathbf{cS}_{O,P}^{X}\mathbf{OH}$, 0.03 mmol) in anhydrous THF (5 mL) at RT under an Ar atmosphere was dropwise added a suspension of sodium *tert*-butoxide (4 mg, 0.045 mmol) in anhydrous THF (1 mL). The mixture was cooled to 0 °C and a solution of **F′** (8 mg, 0.03 mmol) was added dropwise. Then, the mixture was stirred at RT until the reaction had gone to completion. The resulting suspension was diluted with CH_2Cl_2 (10 mL) and water (10 mL) was added. The organic phase was separated, dried over $MgSO_4$, and evaporated under reduced pressure. The crude product was recovered by either preparative HPLC or by precipitation with acetone (2 mL).

$\mathbf{cS}_{P}\mathbf{F}$: Prepared by preparative HPLC (A/B, 80:20), yellow solid (8 mg, 46% yield); ^{1}H NMR (300 MHz, $CDCl_3$, 25 °C): $\delta = 7.77$ (s, 1H), 7.64 (d, $J = 2$ Hz, 1H), 7.63 (d, $J = 9$ Hz, 1H), 7.37 (d, $J = 8$ Hz, 2H), 7.33 (s, 1H), 7.32 (dd, $J = 9$, 2 Hz, 1H), 7.03 (d, $J = 8$ Hz, 1H), 6.67 (s, 1H), 5.50 (s, 2H), 5.19 (s, 2H), 3.97 (s, 3H), 3.96 ppm (s, 3H); MS (ES+): m/z: 597.1 $[M+Na]^+$; HRMS (ES+): m/z calcd for $C_{27}H_{21}F_3N_2NaO_9$ $[M+Na]^+$: 597.1097, found 597.1091.

$\mathbf{cS}_{O}^{1N}\mathbf{F}$: Prepared by precipitation from acetone; yellow solid (5 mg, 30% yield); ^{1}H NMR (300 MHz, [D$_7$]DMF, 25 °C): $\delta = 10.54$ (s, 1H), 8.23 (s, 1H), 7.75–7.69 (m, 4H), 7.54–7.45 (m, 3H), 6.84 (s, 1H), 5.58 (s, 2H), 5.45 (s, 2H), 3.98 (s, 3H), 3.93 ppm (s, 3H); MS (ES+): m/z 576.14 $[M+H]^+$; HRMS (ES+): m/z calcd for $C_{26}H_{21}F_3N_3O_9$: 576.1230 $[M+H]^+$; found: 576.1224.

$\mathbf{cS}_{P}^{1N}\mathbf{F}$: Prepared by precipitation from acetone; yellow solid (7 mg, 40% yield); ^{1}H NMR (300 MHz, [D$_7$]DMF, 25 °C): $\delta = 10.54$ (s, 1H), 8.43 (s, 1H), 7.80–7.70 (m, 4H), 7.60–7.40 (m, 3H), 6.87 (s, 1H), 5.57 (s, 2H),

5.26 (s, 2H), 3.98 ppm (s, 6H); MS (ES+): *m/z*: 576.2 $[M+H]^+$; HRMS (ES+): *m/z* calcd for $C_{26}H_{21}F_3N_3O_9$: 576.1230 $[M+H]^+$; found: 576.1224.

cS$^{1N}_{O}$F: Prepared by precipitation from acetone; yellow solid (5 mg, 30% yield); ^{1}H NMR (300 MHz, [D$_7$]DMF, 25 °C): $\delta = 10.59$ (s, 1H), 8.57 (s, 1H), 8.33 (s, 1H), 7.77–7.70 (m, 3H), 7.57–7.51 (m, 3H), 6.87 (s, 1H), 5.68 (s, 2H), 5.40 (s, 2H), 4.00 (s, 3H), 3.96 ppm (s, 3H); MS (ES+): *m/z*: 576.09 $[M+H]^+$; HRMS (ES+): *m/z* calcd for $C_{26}H_{21}F_3N_3O_9$: 576.1230 $[M+H]^+$; found: 576.1224.

cS$^{2N}_{P}$F: Prepared by preparative HPLC (A/B, 70:30); yellow solid (5 mg, 30% yield); ^{1}H NMR (300 MHz, $CDCl_3$, 25 °C): $\delta = 8.52$ (s, 2H), 7.78 (s, 1H), 7.67 (d, $J = 2$ Hz, 1H), 7.63 (d, $J = 9$ Hz, 1H), 7.32 (dd, $J = 9$, 2 Hz, 1H), 7.23 (s, 1H), 6.67 (s, 1H), 5.50 (s, 2H), 5.18 (s, 2H), 3.97 (s, 3H), 3.96 ppm (s, 3H); MS (ES+): *m/z*: 577.14 $[M+H]^+$; HRMS (ES+): *m/z* calcd for $C_{25}H_{20}F_3N_4O_9$: 577.1182 $[M+H]^+$; found: 577.1177.

cS$^{2N}_{O}$F: Prepared by preparative HPLC (A/B, 70:30); yellow solid (6 mg, 35% yield); ^{1}H NMR (300 MHz, $CDCl_3$, 25 °C): $\delta = 8.41$ (s, 1H), 7.69 (s, 1H), 7.67 (d, $J = 2$ Hz 1H), 7.63 (d, $J = 9$ Hz, 1H), 7.32 (dd, $J = 9$, 2 Hz, 1H), 7.11 (s, 1H), 6.67 (s, 1H), 5.79 (s, 2H), 5.16 (s, 2H), 3.99 (s, 3H), 3.96 ppm (s, 3H); MS (ES+): *m/z*: 591.1 $[M+H]^+$; HRMS (ES+): *m/z* calcd for $C_{26}H_{22}F_3N_4O_9$: 591.1339 $[M+H]^+$; found: 591.1333.

Analytical Solutions

All of the experiments were performed in MeCN/0.1 M Britton–Robinson buffer (1:1, v/v).[18] All of the solutions were prepared by using water that was purified through a Direct-Q 5 (Millipore, Billerica, MA) system.

UV/Vis Absorption

UV/Vis absorption spectra were recorded in quartz cuvettes (1 cm × 1 cm, Hellma) on a diode-array UV/Vis spectrophotometer (Cary 300, Agilent, Thermo Scientific) at 298 K. Molar absorption coefficients were extracted whilst checking the validity of the Beer–Lambert law.

Steady-State Fluorescence Emission

Corrected fluorescence spectra upon one-photon excitation were recorded on a Photon Technology International QuantaMaster QM-1 spectrofluorimeter (PTI, Monmouth Junction, NJ) that was equipped with a Peltier cell holder (TLC50, Quantum Northwest, Shoreline, WA). Solutions for the fluorescence measurements were adjusted to concentrations such that the absorption maximum was about 0.15 at the excitation wavelength.

Irradiation Experiments

One-photon-irradiation experiments were performed on the spectrofluorimeter with or without pH variation. Irradiations were performed by using a filtered 75 W Xe lamp at several slit widths on 400 μL samples in quartz fluorescence cuvettes (0.2 cm × 1 cm, Hellma) under constant stirring. The incident-light intensities were calibrated with α-(4-dimethylaminophenyl)-*N*-phenylnitrone actinometer according to a literature procedure.[19] Typical integral incident-light intensities were within the range 1×10^{-9} Ein s^{-1}.

Acknowledgements

This work was supported by France Bioimaging and by the ANR Blanc 2010 (Kituse).

[1] P. L. Carl, P. K. Chakravarty, J. A. Katzenellenbogen, *J. Med. Chem.* **1981**, *24*, 479–480.
[2] a) C. A. Blencowe, A. T. Russell, F. Greco, W. Hayes, D. W. Thornthwaite, *Polym. Chem.* **2011**, *2*, 773–790; b) A. D. Wong, M. A. DeWit, E. R. Gillies, *Adv. Drug Delivery Rev.* **2012**, *64*, 1031–1045; c) R. E. Wang, F. Costanza, Y. Niu, H. Wu, Y. Hu, W. Hang, Y. Sun, J. Cai, *J. Controlled Release* **2012**, *159*, 154–163.
[3] a) J. C. Florent, X. Dong, G. Gaudel, S. Mitaku, C. Monneret, J. P. Gesson, J. C. Jacquesy, M. Mondon, B. Renoux, S. Andrianomenjanahary, S. Michel, M. Koch, F. Tillequin, M. Gerken, J. Czech, R. Straub, K. Bosslet, *J. Med. Chem.* **1998**, *41*, 3572–3581; b) B. E. Toki, C. G. Cerveny, A. F. Wahl, P. D. Senter, *J. Org. Chem.* **2002**, *67*, 1866–1872; c) M. Shamis, H. N. Lode, D. Shabat, *J. Am. Chem. Soc.* **2004**, *126*, 1726–1731; d) R. J. Amir, M. Popkov, R. A. Lerner, C. F. Barbas III., D. Shabat, *Angew. Chem. Int. Ed.* **2005**, *44*, 4378–4381; *Angew. Chem.* **2005**, *117*, 4452–4455; e) A. Gopin, S. Ebner, B. Attali, D. Shabat, *Bioconjugate Chem.* **2006**, *17*, 1432–1440; f) Y. Zhang, Q. Yin, L. Yin, L. Ma, L. Tang, J. Cheng, *Angew. Chem. Int. Ed.* **2013**, *52*, 6435–6439; *Angew. Chem.* **2013**, *125*, 6563–6567.
[4] a) N. H. Ho, R. Weissleder, C. H. Tung, *ChemBioChem* **2007**, *8*, 560–566; b) T. Chauvin, P. Durand, M. Bernier, H. Meudal, B. T. Doan, F. Noury, B. Badet, J. C. Beloeil, E. Tóth, *Angew. Chem. Int. Ed.* **2008**, *47*, 4370–4372; *Angew. Chem.* **2008**, *120*, 4442–4444; c) E. Sella, D. Shabat, *J. Am. Chem. Soc.* **2009**, *131*, 9934–9936; d) G. C. van de Bittner, E. A. Dubikovskaya, C. R. Bertozzi, C. J. Chang, *Proc. Natl. Acad. Sci. USA* **2010**, *107*, 21316–21321; e) M. S. Baker, S. T. Phillips, *J. Am. Chem. Soc.* **2011**, *133*, 5170–5173; f) G. G. Lewis, M. J. Ditucci, S. T. Phillips, *Angew. Chem. Int. Ed.* **2012**, *51*, 12707–12710; *Angew. Chem.* **2012**, *124*, 12879–12882; g) H. Xie, J. Mire, Y. Kong, M. Chang, H. A. Hassounah, C. N. Thornton, J. C. Sacchettini, J. D. Cirillo, J. Rao, *Nat. Chem.* **2012**, *4*, 802–809; h) O. Redy, D. Shabat, *J. Controlled Release* **2012**, *164*, 276–282; i) F. Touti, P. Maurin, J. Hasserodt, *Angew. Chem. Int. Ed.* **2013**, *52*, 4654–4658; *Angew. Chem.* **2013**, *125*, 4752–4756; j) J. Sloniec, U. Resch-Genger, A. Hennig, *J. Phys. Chem. B* **2013**, *117*, 14336–14344.
[5] a) M. P. Hay, B. M. Sykes, W. A. Denny, C. J. O'Connor, *J. Chem. Soc. Perkin Trans. 1* **1999**, 2759–2770; b) E. E. Weinert, R. Dondi, S. Colloredo-Melz, K. N. Frankenfield, C. H. Mitchell, M. Freccero, S. E. Rokita, *J. Am. Chem. Soc.* **2006**, *128*, 11940–11947; c) K. M. Schmid, L. Jensen, S. T. Phillips, *J. Org. Chem.* **2012**, *77*, 4363–4374; d) J. S. Robbins, K. M. Schmid, S. T. Phillips, *J. Org. Chem.* **2013**, *78*, 3159–3169; e) K. M. Schmid, S. T. Phillips, *J. Phys. Org. Chem.* **2013**, *26*, 608–610.
[6] a) R. Labruère, A. Alouane, T. Le Saux, I. Aujard, P. Pelupessy, A. Gautier, S. Dubruille, F. Schmidt, L. Jullien, *Angew. Chem. Int. Ed.* **2012**, *51*, 9344–9347; *Angew. Chem.* **2012**, *124*, 9478–9481; b) A. Alouane, R. Labruère, T. Le Saux, I. Aujard, S. Dubruille, F. Schmidt, L. Jullien, *Chem. Eur. J.* **2013**, *19*, 11717–11724; c) Record of records, *Chem. Rec.* **2013**, *13*, 456–479.
[7] R. Perry-Feigenbaum, P. S. Baran, D. Shabat, *Org. Biomol. Chem.* **2009**, *7*, 4825–4828.
[8] Heterocyclic self-immolative linkers and conjugates, PCT WO 2005/082023A2 (09.09.2005); heterocyclic self-immolative linkers and conjugates, US 2009/0041791A1 (12.02.2009); heterocyclic self-immolative linkers and conjugates, US 7,754,681 B2 (13.07.2010).
[9] R. Jasuja, J. Keyoung, G. P. Reid, D. R. Trentham, S. Khan, *Biophys. J.* **1999**, *76*, 1706–1719.
[10] H.-J. Jin, J. Lu, X. Wu, *Bioorg. Med. Chem.* **2012**, *20*, 3465–3469.
[11] a) M. Caplow, *J. Am. Chem. Soc.* **1968**, *90*, 6795–6803; b) S. L. Johnson, D. L. Morrison, *J. Am. Chem. Soc.* **1972**, *94*, 1323–1334.
[12] I. Aujard, C. Benbrahim, M. Gouget, O. Ruel, J.-B. Baudin, P. Neveu, L. Jullien, *Chem. Eur. J.* **2006**, *12*, 6865–6879.
[13] S. J. Nara, L. Valgimigli, G. F. Pedulli, D. A. Pratt, *J. Am. Chem. Soc.* **2010**, *132*, 863–872.
[14] a) S. F. Mason, *J. Chem. Soc.* **1958**, 674–685; b) D. J. Brown, *Pyrimidines and their Benzo Derivatives* in *Comprehensive Heterocyclic Chemistry* (Eds.: A. R. Katritzky, C. W. Rees), Pergamon Press, Oxford, **1984**.
[15] D. J. Brown, L. N. Short, *J. Chem. Soc.* **1953**, 331–337.
[16] A. R. Katritzky, A. F. Pozharskii, *Handbook of Heterocyclic Chemistry*, 2nd ed., Pergamon Press, Oxford, **2000**.
[17] H. Y. Lee, X. Jiang, D. Lee, *Org. Lett.* **2009**, *11*, 2065–2068.
[18] C. Frugoni, *Gazz. Chim. Ital.* **1957**, *87*, 403–407.
[19] P. F. Wang, L. Jullien, B. Valeur, J.-S. Filhol, J. Canceill, J.-M. Lehn, *New J. Chem.* **1996**, *20*, 895–907.

Received: January 9, 2014
Published online: ■■ ■■, 0000

Photoactivation

Ahmed Alouane, Raphaël Labruère, Katherine J. Silvestre, Thomas Le Saux, Frédéric Schmidt,* Ludovic Jullien**

Disassembly Kinetics of Quinone-Methide-Based Self-Immolative Spacers that Contain Aromatic Nitrogen Heterocycles

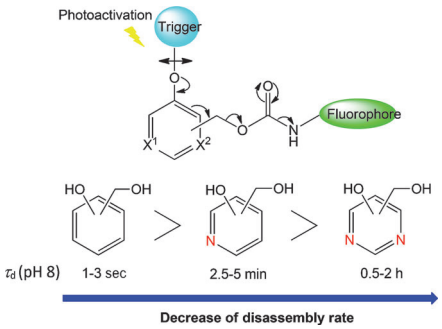

Burn rubber: Kinetic analysis of the pH-dependent disassembly of self-immolative spacers that contain aromatic nitrogen heterocycles was performed. Electron-poor pyrimidine cores exhibited the longest disassembly times. This study confirms the trend that electron-rich aryl cores accelerate self-immolation.